Formation of Water Networks on Anionic Perylene

Heinrich Salzmann,[a,b] *Natalie LeMessurier,*[b] *Joel D. Eaves,*[b] *and J. Mathias Weber*[a,b]*

[a] JILA, University of Colorado, Boulder, CO 80309-0440, USA

[b] Department of Chemistry, University of Colorado, Boulder, CO 80309-0215, USA

TOC Graphic

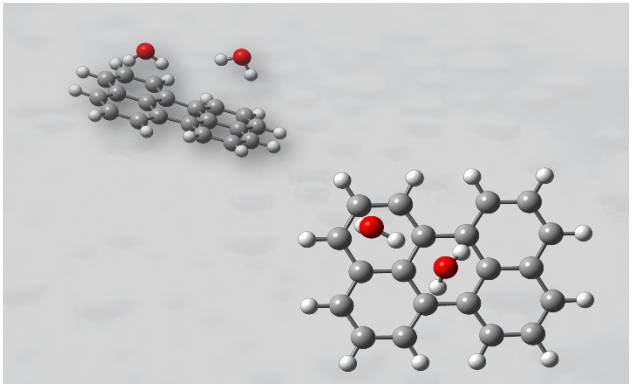

ABSTRACT. We present infrared photodissociation spectra of hydrated perylene anion clusters with up to four water molecules, as well as electronic structure calculations based on density functional theory. Water molecules form weak hydrogen bonds to the π system of the perylene anion. For clusters with more than one water molecule, water-water hydrogen bonds are formed, which generally appear to be stronger than water-π hydrogen bonds, especially for the trihydrate and tetrahydrate. The resulting water networks exist as water subclusters on the surface of the carbon frame of perylene. We observe temperature dependent dynamic effects, which highlight large amplitude motions of the water network and the shallowness of the potential energy surfaces governing the structures of these clusters.

Introduction

Polyaromatic hydrocarbons (PAHs) are a very important class of chemical species. They are common environmental pollutants from sources such as biomass burning and vehicle emissions, and they have carcinogenic effects in humans.[1-4] PAHs are ubiquitous in astrochemistry, where they are estimated to contain up to 20% of all carbon in the universe.[5-10] While cationic and neutral PAHs are likely to be important molecular species in regions with high radiation flux,[9, 10] anionic PAHs are thought to play an important role in dark astrochemical environments as electron sinks and carriers of negative charge.[11, 12] The reactivity and formation mechanisms of small PAHs have recently gained increased interest, since high abundances of pyrene have been calculated based on samples from the asteroid Ryugu[5] and on the detection of 1- and 2-cyanopyrene in the cold interstellar cloud TMC-1.[13, 14]

While PAHs themselves are interesting in their own right, their interaction with water is of particular importance, e.g., in ice grains in interstellar clouds and comets, and in PAH environmental chemistry. In a technology context, interactions of water with aromatic systems are relevant for applications of graphene-based materials in aqueous environments.[15-18] As a consequence, better understanding and modeling of the interactions between water and aromatic π-systems are highly desirable.

In principle, these interactions are encoded in the infrared (IR) active OH stretching vibrations of water molecules in contact with a PAH molecule. However, the relevant vibrational signatures are challenging to resolve in macroscopic aqueous systems, as the spectroscopic response from bulk water obscures signals from interfaces with PAHs or graphene-like materials. Investigating the interactions of isolated PAHs with few water molecules provides computationally[19-31] and experimentally[20-30, 32, 33] accessible model system for graphene and carbon nanotubes.

Spectroscopy of gas-phase cluster studies conducted *in vacuo* offer a way to investigate molecular geometries and interactions of the relevant cluster constituents in the absence of complications from bulk effects, providing insight into intermolecular hydrogen bonding (H-bonding) motifs. Multiple spectroscopic approaches have been used to study the microhydration of cationic,[26, 27] neutral,[20-23, 25, 28, 29, 31, 32] and anionic[11, 24, 30, 33] PAH-water clusters. One approach is to combine mass spectrometry and IR spectroscopy for vibrational spectroscopy of microhydrated clusters, which has been applied to PAH-water cluster ions previously[24, 26, 27, 30] and is used in the present work.

The microhydration of PAHs depends strongly on their charge. In cationic PAH-water clusters, the dipole moment of water orients the oxygen atom towards the CH groups on the periphery of the PAH, as exemplified in work by Dopfer and coworkers on naphthalene.[26] A comparatively weak interaction between water and the positively charged aromatic π-system through the lone pairs on O atoms develops only in clusters with at least three water molecules in this case.[27] Experimental and computational studies on neutral PAH-water clusters revealed that water binds loosely to the aromatic π-system through OH···π H-bonds.[20-23, 25, 28, 29, 31, 32, 34] Rotational spectra of phenanthrene-water complexes show signatures of tunneling of the water molecule across the surface of the carbon frame, highlighting the ability of water to move across the π-system.[23, 28, 32] In clusters with more than one water molecule, the water-water interactions are stronger than water-PAH interactions,[20] and clusters with more than two water molecules seem to preferentially form rings.[20, 21, 23, 25, 28]

The interaction between water and the aromatic π-system is significantly stronger in anionic PAH water clusters, where the excess negative charge is delocalized through the π-system. In the case of pyrene-water clusters, one can estimate from photoelectron spectra by Lietard et al.[11] that

the binding energy of the excess electron is stabilized by the presence of a single water molecule by 0.24 eV, as the excess charge in the π system leads to the formation of stronger H-bonds between the PAH and water molecules or water subclusters. For three and four water molecules, these water networks preferentially form rings,[24, 30] reminiscent of the neutral water trimer[35, 36] and tetramer,[37, 38] hydrated neutral PAHs,[20, 21, 23, 25, 28] and hydrated halides.[39, 40] In contrast, the free water trimer anion prefers a chain structure,[41] and both chain and ring isomers are populated in the tetramer anion.[42] In naphthalene-water cluster anions,[24] the water network is constrained by the size of the PAH, destabilizing ring structures and causing coexistence of chain and ring isomers for the trihydrate. The geometric frustration of the water network increases with water network size and is particularly pronounced for five and more water molecules, which form prismatic structures instead of rings.[24] Larger, two-dimensionally extended PAHs like pyrene do not show similar confinement effects at these cluster sizes, making ring structures of the water subcluster the clearly preferred motif.[30] Our previous spectroscopic investigation of argon tagged pyrene water clusters revealed dynamically broadened absorption features associated with OH stretching vibrations,[30, 33] suggesting that the internal energy of the cluster causes water molecules to move across the pyrene surface, and we can expect similar effects in hydrated perylene (Per) anion.

In the present work, we report the IR spectra of hydrated perylene cluster anions with up to four water molecules, acquired by monitoring Ar loss from argon-tagged $Per^{-}\cdot(H_2O)_{1,2}$ and water loss from $Per^{-}\cdot(H_2O)_n$ (n = 1 – 4). We assign structures of the water subclusters by comparing the experimental spectra with calculated spectra of different isomers from density functional theory (DFT), and we discuss the influence of temperature on the structures and spectra.

Methods

Experimental – We prepared cluster ions of the form $Per^{-}\cdot(H_2O)_n\cdot Ar_m$ (n = 1 – 4, m = 0 – 2) using a pulsed supersonic entrainment source, which has been described in detail elsewhere.[24, 30, 33, 43] A pulsed supersonic expansion of neat Ar was generated using an Even-Lavie valve. Water vapor was entrained into the supersonic beam via a second pulsed valve (General Valve Series 9), and Per vapor was entrained from an oven heated to 485±10 K. An electron beam (~800 eV kinetic energy) was focused into the high-density region of the supersonic expansion, generating an electron impact plasma. Attachment of slow, secondary electrons in the plasma created molecular and cluster anions. The anions were accelerated perpendicularly to the expansion using a Wiley-McLaren accelerator and injected into a time-of-flight mass spectrometer. A mass spectrum of the ions formed under typical operating conditions of the ion source is shown in Supporting Information (Figure S1). For the mono- and dihydrate clusters (n = 1, 2), we were able to produce sufficient amounts of Ar-tagged ions to perform IR Ar predissociation spectroscopy. For n = 3 and 4, this was not possible, and we used the untagged $Per^{-}\cdot(H_2O)_n$ ions as targets. Ions with the desired mass-to-charge ratio were mass-selected using an interleaving comb mass gate and irradiated with light from a pulsed, tunable OPO/OPA system (LaserVision, pulse duration 5−7 ns, linewidth ca. 2 cm^{-1}, pulse energy ca. 5−10 mJ). Photon absorption and subsequent intramolecular vibrational redistribution led to fragmentation of the target clusters. For Ar-tagged clusters, fragmentation resulted in the loss of the Ar tags:

$$Per^{-}\cdot(H_2O)_n\cdot Ar_m + h\omega \rightarrow Per^{-}\cdot(H_2O)_n + m\,Ar \quad (1)$$

Spectra of untagged $Per^{-}\cdot(H_2O)_n$ clusters were acquired by monitoring the loss of one water molecule following the reaction

$$Per^{-}\cdot(H_2O)_n + h\omega \rightarrow Per^{-}\cdot(H_2O)_{n-1} + H_2O \quad (2)$$

The abundance of the resulting fragment ions in each case was recorded as a function of the wavenumber of the tunable IR light. Where necessary, a baseline correction was applied to the fragment ion data because the ion fragment signal was prone to drift over the duration of a scan. Anchor points were manually set to define a baseline in the OriginPro Peak Analyzer tool,[44] connected by straight lines. A comparison of the baseline-corrected data with the uncorrected data is shown in Figure S2. The frequency of the light source was calibrated by comparison with a photoacoustic spectrum of water vapor.[45] To obtain an IR photodissociation spectrum from the observed fragment ion intensity, the fragment ion signal was normalized by the number of photons. Multiple spectra collected on different days were averaged to improve the signal-to-noise ratio and ensure reproducibility.

Computational – For each cluster size, several structures were used as starting points for geometry optimization, using DFT as implemented in Gaussian 16,[46] employing the ωB97X-D functional[47] and 6-311G+(d,p)[48, 49] basis sets for all atoms. Exploratory calculations using the B3LYP functional[50] resulted in qualitatively similar results (see Supporting Information). Similar to the case of hydrated pyrene cluster anions, the potential energy surface of $Per^{-}\cdot(H_2O)_n$ clusters is characterized by very flat basins.[30] To obtain well-converged structures, we employed a strict convergence criterion with a root-mean-square force of 10^{-6} H/Å (using the "very-tight" keyword in Gaussian 16). In cases where this geometry optimization strategy still failed, a quadratic convergence criterion was applied. Harmonic frequencies were scaled by 0.9375 to account for anharmonicity, with the scaling factor determined based on the average of the symmetric and anti-symmetric OH stretch of a free water molecule, treated with the same computational methods (3657 cm^{-1} and 3756 cm^{-1}, respectively). To determine partial charges, we used the Merz-Singh-

Kollman electrostatic potential (ESP) method.[51, 52] as in our previous work on anionic hydrated pyrene clusters.[30, 33] Molecular interaction energies were determined from calculations of the counterpoise corrected binding energies of water molecules or water cluster fragments to the perylene anion (see Supporting Information for more details).

Results and Discussion

The IR photodissociation spectra of $Per^{-}\cdot(H_2O)_n\cdot Ar_m$ (n = 1 – 4; m = 0 – 2) in the OH stretching region are shown in Figure 1 (see Supporting Information for a brief discussion of the CH stretching region).

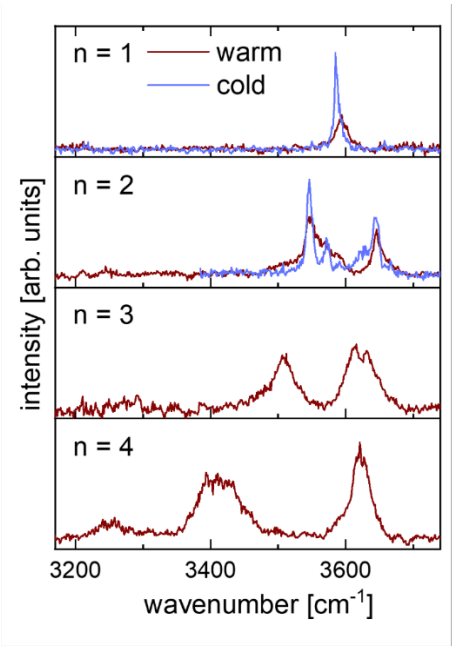

Figure 1. Overview of Per^{-} microhydration, with the number of water molecules (n) indicated in each panel. The blue traces represent spectra acquired by Ar predissociation (with two Ar tags for n = 1 and one Ar tag for n = 2), while the red traces show photodissociation spectra taken by the loss of a single water molecule from the parent cluster. For n = 1 and 2, the spectra of cold and warm clusters are scaled to represent equal integrated peak areas.

Different from the CH stretching absorption features, which are largely unaffected by Ar tagging (see Supporting Information), the OH stretching modes show significant spectral differences between tagged and untagged clusters. The spectra of tagged clusters have significantly narrower lines and as a result exhibit better resolved features than the spectra of the warm clusters. The main difference between tagged and untagged species is their internal energy content. Assessing the internal energy of clusters formed in a supersonic expansion plasma without well-characterized temperature dependent spectroscopic signatures is challenging, and we can only give a qualitative characterization of the tagged clusters as "cold" and the untagged clusters as "warm", with estimated microcanonical temperature equivalents of < 110 K for tagged and < 180 K for untagged clusters (see Supporting Information for details). The difference in internal energy results in a difference in the dynamics of the clusters. As will be discussed in more detail below, the configurational and potential energy landscape for the motion of water molecules and clusters across the surface of a PAH π system is characterized by shallow, broad minima, leading to pronounced dynamic effects, and ultimately result in broadening effects best described by spectral diffusion.[33]

We note that similar to pyrene, Per has a positive adiabatic electron affinity (EA), measured at 0.9730±0.005 eV by Schiedt and Weinkauf.[53] We therefore do not expect photodetachment to play any role in the spectral region relevant for the present work, in contrast to the case of hydrated naphthalene.[24]

The interpretation of the OH stretching region is organized in the following sections from monohydrate to tetrahydrate as the spectral complexity grows with increasing hydration level.

Monohydrate (n = 1)

The photodissociation spectrum of $Per^{-}\cdot H_2O\cdot Ar_m$ (m = 0, 2) in the OH stretching region (Figure 2) is dominated by the signature of the symmetric OH stretching mode (ω_s), which peaks at 3585 cm^{-1} for the Ar tagged cluster and at 3594 cm^{-1} for the untagged cluster. A much weaker feature at 3657 cm^{-1} corresponds to the anti-symmetric OH stretching mode (ω_a) for the cold complex, and the observed splitting between ω_s and ω_a (72 cm^{-1}) is in reasonable agreement with the scaled harmonic calculation (64 cm^{-1}). The bottom panel of Figure 2 displays the calculated spectrum of the lowest energy conformer of $Per^{-}\cdot H_2O$, which we used to identify the absorption features. The spectra calculated for higher energy conformers show no significant differences to that for the lowest energy structure (see Figures S4 and S5 in Supporting Information). The overall pattern of the spectrum is consistent with those previously observed for the monohydrated anions of naphthalene[24] and pyrene.[33] The symmetric OH stretching signature of the cold, Ar-tagged clusters has an asymmetric line shape with a high frequency tail and a full width at half-maximum (FWHM) of 8 cm^{-1}, about 2 cm^{-1} wider than the narrowest features in the CH stretching region. In contrast, the same feature of the warm, untagged $Per^{-}\cdot H_2O$ clusters is significantly broader and slightly blue-shifted compared to the cold spectrum, with a FWHM of 19 cm^{-1}. The absorption feature of the warm clusters is wider and more symmetric in line shape, while the splitting between ω_s and ω_a is smaller in comparison to the splitting observed for the cold clusters. Both OH groups interact with the π-system of the PAH, resulting in a red shift of both ω_s and ω_a from their values in free water, where the symmetric and antisymmetric OH stretching modes are 3657 cm^{-1} and 3756 cm^{-1}. The overall calculated binding energy of the water molecule in $Per^{-}\cdot H_2O$ is 3508 cm^{-1}. Table 1 shows the calculated water-π interaction energies for each cluster size.

Table 1. Calculated Interaction Energies[a]

n	π [cm^{-1}]	water-water [cm^{-1}]
1	3508	-
2[b]	3111(D), 3118 (A)	1492
3[c]	2599	1796
4[c]	2451	2629

[a] see Supporting Information for details.

[b] D = H-bond donor, A = H-bond acceptor.

[c] π interaction energy per water molecule, water-water interaction energy per H-bond, assuming ring conformer.

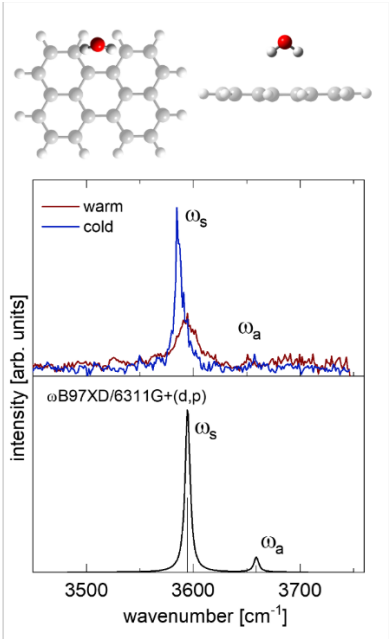

Figure 2. Top: Calculated structure of the lowest energy conformer of $Per^{-}\cdot H_2O$ (red: O; C: gray; H: white; the Per frame has been deemphasized to highlight the water structure). Center: Experimental IR spectra of the OH stretching region for warm $Per^{-}\cdot H_2O$ (red) and cold $Per^{-}\cdot H_2O\cdot Ar_2$ (blue). The spectra of cold and warm clusters are scaled to represent equal integrated peak areas. Bottom: Calculated spectrum of the lowest energy conformer, broadened to 6 cm^{-1} FWHM using a Lorentzian function (individual transitions are shown as vertical lines). See text for labels.

Similar to the case of pyrene monohydrate, the configurational landscape is characterized by shallow, broad minima, leading to pronounced dynamic effects.[33] One of these effects is that the water molecule can likely move across the perylene frame even at low temperature.[33] Another consequence is that thermal motion in the cluster also leads to significant fluctuations regarding the angle between the surface normal and the H-bonded OH group.[33] This fluctuation weakens the H-bond to the π-system compared to its zero K structure, thereby strengthening the bond of the OH group closer to the PAH, and resulting in an asymmetric line shape with a tail on the higher frequency side of the symmetric stretching feature.[33] While the dynamic effects observed here are similar in character to the broadening of the symmetric stretching feature found in monohydrated anionic pyrene, they are less pronounced here, as the FWHM in Ar-tagged hydrated pyrene was about double compared to that observed for perylene monohydrate under similar conditions.[33] We hypothesize that this narrowing effect may be due to the unusual structure of the lowest energy monohydrate conformer, which does not access the π system across the carbon frame, but is straddling the gap between the two naphthalene subunits, and may be less mobile, resulting in less dynamic broadening at low temperature. We note that an alternative explanation would be combination bands involving soft intermolecular vibrational modes. These modes have calculated frequencies of the order of 20-30 cm^{-1}, which is too high to explain the observed effects. Other possibilities would be saturation broadening or broadening effects from multiphoton dissociation. While small saturation effects are possible, we estimate from earlier work on pyrene and its water clusters that the suppression of peak intensities would be no more than 10%. In addition, saturation broadening would impact the width of both tagged and untagged species. We can rule out

significant contributions from multiphoton broadening based on the fragment ion yield and photon fluence in our experiment.

Dihydrate (n = 2)

The addition of a second water molecule to $Per^{-}\cdot H_2O$ leads to water-water interactions. The spectrum of $Per^{-}\cdot(H_2O)_2\cdot Ar$ (Figure 3) shows several well-resolved bands, which are similar to the overall patterns observed in the dihydrate clusters of anionic naphthalene[24] and pyrene.[30] We will use the spectrum of the cold, Ar-tagged cluster to assign the observed vibrational features based on the comparison with relevant isomers of the cluster (Figure 4), since it is significantly better resolved than the analogous spectrum of the warmer $Per^{-}\cdot(H_2O)_2$ cluster. Most of the spectral features can be assigned (bottom panel of Figure 3) to a structure that exhibits a water dimer subcluster, with a H-bond donor and a H-bond acceptor (Figure 4). There are several low-energy structures characterized by such a water dimer subcluster (see Figure S6 in Supporting Information).

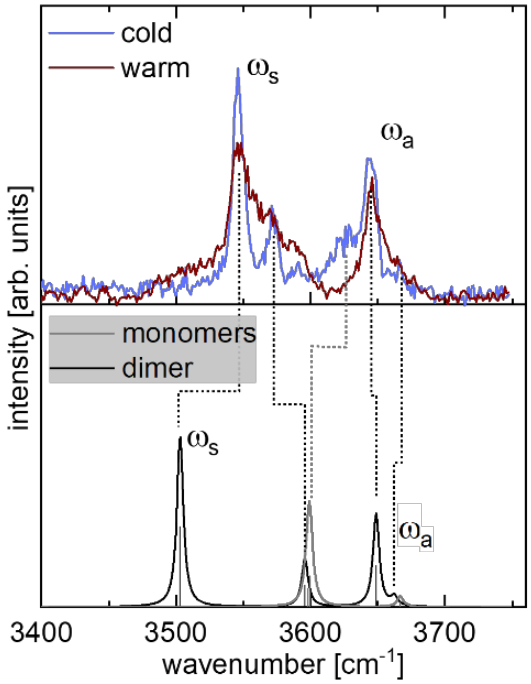

Figure 3. Top panel: IR spectra of $Per^{-}\cdot(H_2O)_2$ (warm, red) and $Per^{-}\cdot(H_2O)_2\cdot Ar_2$ (cold, blue) in the OH stretching region. The spectra of cold and warm clusters are scaled to represent equal integrated peak areas. Bottom panel: Calculated harmonic frequencies of the lowest-energy dimer structure (black) and of a structure with two independent water molecules (grey). The calculated spectra are broadened with a Lorentzian function to 6 cm^{-1} FWHM. The dotted lines visualize the assignment. See text for labels.

The spectrum can be roughly grouped into features that originate from linear combinations of local symmetric (ω_s) and antisymmetric (ω_a) OH stretching motions of the individual water molecules, with the symmetric stretching motions found at lower frequencies (see Table 2). The lowest frequency band at 3546 cm^{-1} corresponds to a normal mode characterized by the in-phase linear combination of the local symmetric stretching modes of the two water molecules, mostly due to the motions of the H-bond donor molecule. We tentatively assign weaker bands at 3572 cm^{-}

[1] and at 3591 cm^{-1} to the out-of-phase linear combination of these two local modes, where the H-bond acceptor carries most of the amplitude, and the two different bands come from two different isomers that are both characterized by a similar water dimer subcluster (see Supporting Information) . We note that an alternative interpretation of the two different bands could involve a combination band of the in-phase linear combination of the symmetric stretching band with a low frequency soft mode of the cluster (there are several candidates of such bands). The intense band at 3644 cm^{-1} has the character of an antisymmetric stretching motion on the H-bond donor molecule combined with a small amplitude in the local symmetric stretching motion on the acceptor molecule. Finally, a weak feature at 3666 cm^{-1} is characterized by antisymmetric OH stretching motions on the acceptor molecule. The two most intense features have significant amplitude in the motion of the OH group involved in the water-water H-bond.

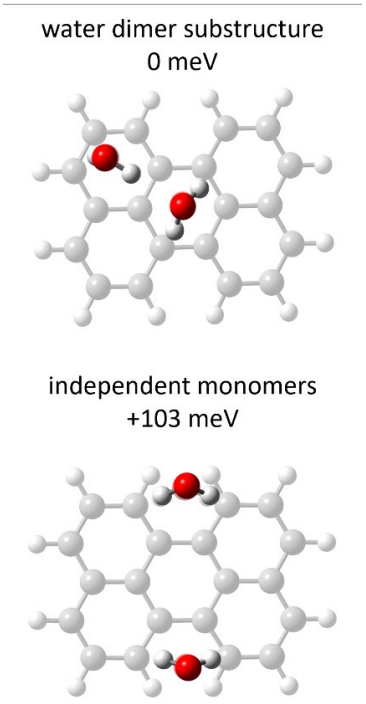

Figure 4. Selected calculated conformations of $Per^{-}\cdot(H_2O)_2$, with relative energies given with each structure. Red: O; C: gray; H: white; the Per frame has been deemphasized to highlight the water substructure.

Table 2. Peak Assignment in the OH Stretching Region of Cold Perylene Dihydrate.

experimental [cm^{-1}]	character	calculated [cm^{-1}]
3546	ω_s in phase (H-bond donor)	3503
3572, 3591	ω_s out of phase (H-bond acceptor)[a]	3584-3596
3627	ω_s (monomers)	3609
3644	ω_a (H-bond donor)	3648
3666	ω_a H-bond acceptor	3663

[a] belonging to different conformers with water dimer subclusters.

The water dimer is generally challenging to treat computationally.[54-56] In the present case, this difficulty is reflected in a significant discrepancy between the calculated and observed splittings of the out-of-phase and in-phase linear combinations of the local symmetric stretching modes; in the experimental spectrum the in-phase and out of phase absorption features are separated by 26 cm^{-1} and 45 cm^{-1} for the bands tentatively attributed to the two different isomers, while the calculated vibrational modes are separated by ca. 90 cm^{-1}.[54-56] The overestimation of the frequency splitting between the symmetric stretching modes in $Per^{-}\cdot(H_2O)_2$ is similar to that in the free water dimer for our own level of theory as well as some higher level calculations from the literature[55] (see Supporting Information Table S3). Despite this discrepancy, we can assign this out-of-phase combination of ω_s based on the overall intensity pattern of the calculated spectra and through the similarity with the spectra of the dihydrate clusters of pyrene[30] and naphthalene.[24] We found this pattern to be robust among various different calculations which showed some frequency dependence on the functional and basis set (see Figure S8 in Supporting Information).

The presence of the Per^- anion results in a significant change in the structure and spectrum of the water dimer subcluster compared to the free, neutral water dimer. The OH groups not engaged in H-bonding in the free water dimer point in opposite directions to optimize dipole-dipole interactions between the two water molecules. In $Per^-\cdot(H_2O)_2$, these OH groups now interact with the π system and therefore point in the same overall direction, straining the water-water interaction in the dimer. At the same time, the frequencies for the different OH oscillators are significantly reordered (see Supporting Information Table S3), since the interaction with the π system weakens the (formerly) free OH bonds. As a result, the spectra of the free and PAH bound water dimer are not directly comparable.

While the weak feature at 3591 cm^{-1} is likely due to another isomer with a dimeric subcluster, the broad peak around 3627 cm^{-1} may have a different origin. We tentatively assign it to isomers with two independent water molecules (bottom panel of Figure 3). Such isomers are significantly higher in energy, (ca. 120 – 130 meV), but could be kinetically trapped in the cold clusters, having either two water molecules on opposing sites or distributed over the two naphthalene-like subunits on the same side of Per^- (see Figure 4 and Supporting Information Figures S6 and S7). The linear combinations of the local symmetric OH stretching modes of the two water molecules would appear close to each other, and the calculations predict a splitting of ca 10 cm^{-1} between them, consistent with the existence of a broad feature containing both signatures. Our interpretation is consistent with the temperature dependence of this feature (see below). We note that we do not observe the signatures of the antisymmetric stretching modes of the independent monomers, and we assume that they are too weak to be noticeable in our experimental data.

The spectrum of the warm cluster appears to mostly represent a broadened version of the spectrum of the cold cluster, which is to be expected, given the dynamic effects that are likely to

appear as a broadening of the individual spectral features of the cluster. Since the signatures of water-water H-bonds persist in the warm clusters, they offer additional insight into the temperature of the cluster, since the internal energy is insufficient to break the H-bond and "melt" the cluster. In experiments on iodide dihydrate clusters by Johnson, Asmis, and coworkers, the water-water H-bond was observed to break at temperatures above 150 K and was largely absent above 180 K.[39] In this context, it is reasonable to assume that the untagged $Per^{-}\cdot(H_2O)_n$ clusters have microcanonical temperature equivalents below 180 K.

The weak feature observed at 3591 cm^{-1} increases in intensity in the spectrum of the warm cluster, which is consistent with an increased thermal population of slightly higher-lying isomers. Interestingly, the broad peak that we assigned above to the signature of two independent monomers disappears in the spectrum of the warm cluster. Since higher internal energy in the cluster would result in more dynamic exploration of the conformational landscape by two independent water molecules, it seems likely that they would encounter each other and undergo H-bond formation. Assuming an upper limit for the temperature in the cold dihydrate cluster similar to that estimated for the monohydrate (see above), the free energy barrier for this reaction would be of the order of k_BT at 109 K, corresponding to ca. 9 meV, which is not unrealistic. We hypothesize that the barrier could be due to crossing from one side of the PAH frame to the other across the single ring connecting the two naphthalene-like subunits. The disappearance of the feature at 3620 – 3630 cm^{-1} in the spectrum of the warm dihydrate cluster is consistent with our tentative assignment above.

Different from the present work, no spectroscopic evidence of kinetically frozen independent water molecules has been found in anionic pyrene and naphthalene water clusters,[24, 30] and previous work on monohydrated, Ar-tagged anionic pyrene, using molecular dynamics, suggested that the water molecule freely explores the entire surface of pyrene.[33] The observation of this

feature in cold perylene dihydrate anion clusters may be due to the narrowness of the bridge between the two naphthalene subunits of perylene, reducing the effective space for roaming of a water molecule across the surface of the PAH. Molecular dynamics simulations of hydrated perylene anions would be highly desirable to investigate this effect.

The calculated interaction energies for the dihydrate (see Table 1) show that the interaction energies of the two water molecules with the π system are very similar, although the H-bond donor molecule of the dimeric subcluster forms one π-H-bond, while the acceptor forms two π-H-bonds. It is important to note that the water-π interaction energies contain contributions from dispersion and polarization interactions (e.g., from the OH group in the water-water H-bond) in addition to contributions from π-H-bond formation. As a result, the water-π interaction energies can be significantly higher than the underlying H-bond interaction energies. The calculated water-water interaction energy at 1492 cm^{-1} is slightly lower than typical calculated binding energies of the neutral water dimer[57] (ca. 21 kJ/mol ≈ 1750 cm^{-1}).

Trihydrate (n = 3)

As mentioned above, the larger clusters in this study were only formed without Ar tagging in amounts sufficient for spectroscopic investigation, in contrast to earlier work on naphthalene[24] and pyrene.[30] We attribute these challenges to the higher melting temperature[58] of Per (551 K) compared to naphthalene (353 K) and pyrene (424 K), which is reflected in the need for higher oven temperatures to create sufficient vapor pressure in the ion source. As a consequence, the internal energy of the clusters is sufficiently high to suppress the formation of Ar tagged species.

The experimental and calculated spectrum of $Per^{-}\cdot(H_2O)_3$ and the lowest energy isomer are shown in Figure 5. Similar to trihydrates of naphthalene[24] and pyrene,[30] the most stable structural

motif is a homodromic ring, where each water molecule acts as both H-bond donor and acceptor, reminiscent of the structure of the neutral water trimer[35-37] and the structures of neutral PAH trihydrates.[20, 21, 23, 25, 28] Different from these neutral species, all OH groups that are not involved in H-bonding within the water network form H-bonds to the negatively charged π-system of the PAH, consistent with the stronger OH-π interaction expected for the anionic systems. The features in the OH stretching region match the simulated spectrum of such a ring motif. Similar to the dihydrate, the lower frequency group of features are derived from linear combinations of the symmetric stretching modes of the local water molecules, while the higher frequency group belongs to linear combinations of the local antisymmetric modes. While this overall characteristic of the local modes persists, we note that the oscillation amplitudes of the OH groups in each water molecule are significantly different due to the breaking of the local symmetry of each water molecule, leading to a partial localization of the oscillation in the OH groups within the ring or to the π system, respectively.

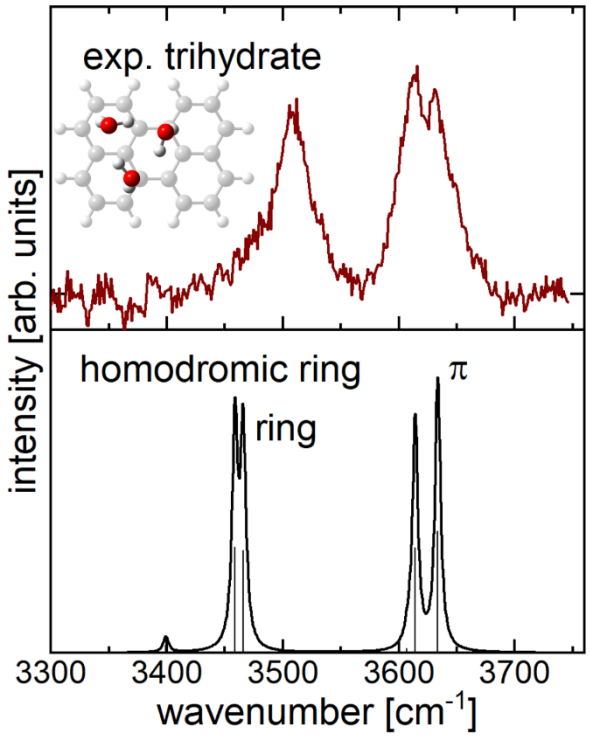

Figure 5. Top panel: Experimental IR spectrum of $Per^{-}\cdot(H_2O)_3$. Bottom panel: Calculated IR spectrum and structure of the lowest energy structure of $Per^{-}\cdot(H_2O)_3$. The calculated spectrum is broadened to 6 cm^{-1} using a Lorentzian function. Red: O; C: gray; H: white; the Per frame has been deemphasized to highlight the water substructure.

The broad absorption feature with a peak at 3506 cm^{-1} contains the unresolved signatures of two normal modes where the oscillation amplitudes are primarily localized within the water ring, and two of the three OH groups oscillate out of phase with the third. A weaker feature, generated by the analogous all-in-phase linear combination, is part of the low-frequency side of this feature. In contrast, the absorption features at 3612 cm^{-1} and 3633 cm^{-1} are attributed to OH oscillations that predominantly involve the OH groups in H-bonds to the π-system. Table 3 summarizes the peak assignments for the trihydrate.

Table 3. Peak Assignment in the OH Stretching Region of Cold Perylene Trihydrate.

experimental [cm^{-1}]	character	calculated [cm^{-1}]
3506	ω_s (water-water H-bonds)	3460, 3466
3612	ω_a (π-H-bonds)	3615
3633	ω_a (π-H-bonds)	3633

Our assignment indicates that the OH stretching modes associated with water-water H-bonds occur at lower frequencies than those linked to water-ion interactions, implying that the H-bonds within the water network are stronger than ionic H-bonds. This ordering of H-bond strength is similar to other anionic hydrated PAHs,[24, 30] but contrasts with findings in many other anionic water complexes, such as halide-water interactions.[40, 59] The different energetic ordering in hydrated PAH anion clusters is due to their comparatively large size and the concomitant delocalization and low density of the excess charge in the π-system.[24, 30] We note that the calculated interaction energies for the trihydrate (see Table 1) seem to contradict the energetic ordering of H-bonding interactions inferred from the spectrum, since each water molecule is forming one π-H-bond, and is calculated to have 2599 cm^{-1} average water-π interaction energy, greater than the calculated average water-water interaction energy at 1796 cm^{-1}. However, as mentioned above, the contributions from H-bonding are only a part of the water-π interaction energy. The calculated water-water interaction energy for the trihydrate is higher than that for the dihydrate, pointing towards significant cooperative effects known to exist in the underlying water ring motifs.[54]

There is no spectroscopic evidence to suggest that other structural motifs, such as chains (Figure S10 in Supporting Information) are significantly populated. However, minor contributions that are masked by the large width of the ring signatures cannot be entirely ruled out.

Tetrahydrate (n=4)

The OH stretching spectrum of untagged $Per^{-}\cdot(H_2O)_4$ exhibits a pattern similar to that of $Per^{-}\cdot(H_2O)_3$, as discussed above. Dominating the spectrum represented in Figure 6 are two broad, prominent features, whose line shapes indicate that they contain several unresolved transitions. One of these features forms a plateau ranging from 3380 cm^{-1} to 3445 cm^{-1}, while the other shows a peak at 3623 cm^{-1} and partially resolved substructures. The calculated frequencies of a homodromic four-membered ring structure match the spectral patterns of these two dominant absorption bands, indicating that four-membered rings are the predominant binding motif in $Per^{-}\cdot(H_2O)_4$ clusters.

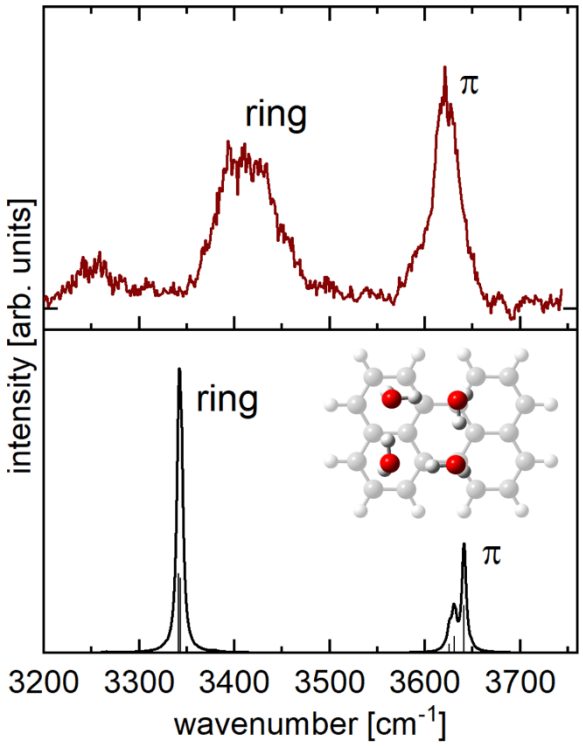

Figure 6. Experimental spectrum (top panel) and calculated structure and frequencies of lowest energy structure of $Per^{-}\cdot(H_2O)_4$ (bottom). The calculated spectrum is broadened by a Lorentzian function with a FWHM of 6 cm^{-1}. Red: O; C: gray; H: white; the Per frame has been deemphasized to highlight the water substructure.

We also explored higher-energy binding motifs, such as a three-membered water ring with a water adduct, and we report these structures and their calculated spectra in Figures S11 and S12 in Supporting Information. Similar to the case of $Per^{-}\cdot(H_2O)_3$, there is no spectroscopic evidence of populations in these higher-energy conformations, but we cannot rule out the possibility of minor contributions that are not spectroscopically resolved.

The lower frequency feature corresponds to modes where the main contributions to the overall amplitude are derived from linear combinations of the local symmetric stretching modes, with OH stretching motions primarily located within the water ring. Different from the trihydrate case, some

of the transitions in this group of features have small amplitude contributions from local antisymmetric modes. The set of features at 3623 cm^{-1} is attributed to OH oscillations associated with the ionic H-bonds with the π-system, mostly originating from linear combinations of the analogous local antisymmetric stretching modes.

Both absorption features contain multiple unresolved transitions. The main discrepancy between calculated frequencies and the observed spectrum are the OH stretching modes primarily located in the water ring, which are predicted as a single intense feature at 3385 cm^{-1} but appear significantly broader feature in the experimental spectrum spanning from 3380 cm^{-1} to 3445. At high internal energies, fluctuations in the structure of the ring will dynamically modify the H-bonding interaction. As a consequence of the greater strength of the water-water H-bonds compared to the π-H-bonds, the frequency positions of the corresponding modes are more sensitive to thermal deformation of the water ring than the modes encoding the water-π interactions, resulting in an overall wider feature.

Below the OH stretching vibrations is a broad absorption feature spanning from 3240 cm^{-1} to 3270 cm^{-1} which is not recovered in harmonic frequency calculations. We assign this feature to overlapping overtones and combination bands of the four water bending modes (calculated at 1594 cm^{-1}, 1598 cm^{-1}, 1602 cm^{-1}, 1612 cm^{-1}), whose intensities are enhanced through Fermi resonances with the fundamental transitions of the symmetric OH stretching modes. While the absorption features belonging to the water bending overtones and combination bands are in the same spectral region for smaller cluster sizes, they are much weaker in intensity, since the symmetric stretching modes of the water molecules are at much higher frequencies than for the tetrahydrate, resulting in much less intensity borrowing. We have observed similar absorption features belonging to the

overtone of the water bending modes in anionic pyrene water clusters.[30] Table 4 summarizes the assignments for the tetrahydrate.

The calculated interaction energies (Table 1) show a strong increase in the water-water interaction energy for the tetrahydrate, probably reflecting a lower geometric strain of the H-bonding network in the ring, and an increase in cooperativity through proton delocalization.[54]

Table 4. Peak Assignment in the OH Stretching Region of Cold Perylene Tetrahydrate.

experimental [cm^{-1}]	character	calculated [cm^{-1}]
3240 – 3270	2 quanta in water bending modes	3559 – 3466
3380 – 3445	ω_s (water-water H-bonds)	3385
3623	ω_a (π-H-bonds)	3633

Conclusion

We have investigated the hydration of anionic Per with clusters $Per^{-}\cdot(H_2O)_n\cdot Ar_m$ (n = 1 – 4, m = 0 – 2) using infrared photodissociation spectroscopy in the OH stretching region. The OH stretching pattern encodes structural information about H-bonding between the water molecules as well as between water molecules and the π-system of Per^{-}, revealing evidence of H-bonds between water molecules for n = 2, as well as the formation of water rings for n = 3 and 4. Water–water H-bonds are stronger than the ionic H-bonds between the water molecules and the delocalized charge on the Per-π system, especially for n = 3 and 4. The potential energy surface of the mono- and dihydrate is shallow, allowing for the existence of multiple energetically accessible conformers. For n = 1 and 2, the lowest-energy structures are closely spaced in energy and differ

primarily in the location of the ionic H-bonds on the perylene surface. In the argon-tagged $n = 2$ cluster, spectroscopic evidence suggests the presence of a higher-energy isomer that is kinetically frozen. For larger water networks ($n = 3$ and 4), homodromic water rings emerge as the dominant binding motif, which undergo significant thermal deformations, leading to broad spectroscopic features. Comparing the current results on hydrated Per anion with previous work on other PAHs, it becomes clear that the size and the shape of the PAH has a subtle influence on the spectra of the hydrated clusters, showing differences in dynamic effects as well as the presence or absence of kinetically frozen water network isomers.

ASSOCIATED CONTENT

Supporting Information. The following files are available free of charge:

File 1 (PDF): Mass spectrum of hydrated anionic perylene clusters; comparison of data with and without baseline correction; discussion of CH stretching vibrations; spectra of the CH stretching region; calculated partial charges within water subcluster; experimental and calculated spectra of Per- monohydrate; geometry optimized conformers of Per- monohydrate; experimental and calculated spectra of Per- dihydrate conformers and isomers; geometry optimized conformers of Per- dihydrate; harmonic spectrum of $Per^{-}\cdot(H_2O)_2$ calculated with various methods; experimental and calculated spectra of Per^{-} trihydrate; geometry optimized conformers of Per^{-} trihydrate; experimental and calculated spectra of Per^{-} tetrahydrate; geometry optimized conformers of Per^{-} tetrahydrate; and atomic coordinates of geometry optimized $Per^{-}\cdot(H_2O)_n$ (n = 1 – 4).

File 2 (PPTX): OH stretching vibrational modes of $Per^{-}\cdot(H_2O)_n$ (n = 2 – 4).

AUTHOR INFORMATION

Corresponding Author

*weberjm@jila.colorado.edu

ACKNOWLEDGMENT

J.M.W. thanks Prof. Mark A. Johnson for sharing his thoughts on the behavior of water networks in clusters (among many other things) throughout the past 25 years. We gratefully acknowledge support from the Department of Energy, Office of Basic Energy Sciences, under award no. DE-SC0021387. This work utilized the Alpine high-performance computing resource at the University of Colorado Boulder. Alpine is jointly funded by the University of Colorado Boulder, the University of Colorado Anschutz, Colorado State University, and with support from NSF grants OAC-2201538 and OAC-2322260.

REFERENCES

(1) Yunker, M. B.; Macdonald, R. W.; Vingarzan, R.; Mitchell, R. H.; Goyette, D.; Sylvestre, S. PAHs in the Fraser River basin: a critical appraisal of PAH ratios as indicators of PAH source and composition. *Org. Geochem.* **2002**, *33*, 489-515.

(2) Moorthy, B.; Chu, C.; Carlin, D. J. Polycyclic Aromatic Hydrocarbons: From Metabolism to Lung Cancer. *Toxicol. Sci.* **2015**, *145*, 5-15.

(3) Srogi, K. Monitoring of environmental exposure to polycyclic aromatic hydrocarbons: a review. *Environ. Chem. Lett.* **2007**, *5*, 169-195.

(4) Manzetti, S. Polycyclic Aromatic Hydrocarbons in the Environment: Environmental Fate and Transformation. *Polycycl. Aromat. Compd.* **2013**, *33*, 311-330.

(5) Zeichner, S. S.; Aponte, J. C.; Bhattacharjee, S.; Dong, G.; Hofmann, A. E.; Dworkin, J. P.; Glavin, D. P.; Elsila, J. E.; Graham, H. V.; Naraoka, H.; et al. Polycyclic aromatic hydrocarbons in samples of Ryugu formed in the interstellar medium. *Science* **2023**, *382*, 1411-1416.

(6) Chabot, M.; Béroff, K.; Dartois, E.; Pino, T.; Godard, M. Coulomb explosion of polycyclic aromatic hydrocarbons induced by heavy cosmic rays: carbon chains production rates. *ApJ* **2019**, *888*, 17.

(7) Dwek, E.; Arendt, R.; Fixsen, D.; Sodroski, T.; Odegard, N.; Weiland, J.; Reach, W.; Hauser, M.; Kelsall, T.; Moseley, S. Detection and characterization of cold interstellar dust and polycyclic aromatic hydrocarbon emission, from COBE observations. *ApJ* **1997**, *475*, 565.

(8) Habart, E.; Natta, A.; Krügel, E. PAHs in circumstellar disks around Herbig Ae/Be stars. *A&A* **2004**, *427*, 179-192.

(9) Tielens, A. G. G. M. Interstellar Polycyclic Aromatic Hydrocarbon Molecules*. *Annu. Rev. Astron. Astrophys.* **2008**, *46*, 289-337.

(10) Tielens, A. G. G. M. The molecular universe. *Rev. Mod. Phys* **2013**, *85*, 1021-1081.

(11) Lietard, A.; Verlet, J. R. R. Effect of Microhydration on the Temporary Anion States of Pyrene. *J. Phys. Chem. Lett.* **2022**, *13*, 3529-3533.

(12) Wakelam, V.; Herbst, E. Polycyclic aromatic hydrocarbons in dense cloud chemistry. *ApJ* **2008**, *680*, 371.

(13) Wenzel, G.; Cooke, I. R.; Changala, P. B.; Bergin, E. A.; Zhang, S.; Burkhardt, A. M.; Byrne, A. N.; Charnley, S. B.; Cordiner, M. A.; Duffy, M.; et al. Detection of interstellar 1-cyanopyrene: A four-ring polycyclic aromatic hydrocarbon. *Science **2024**, 386*, 810-813.

(14) Wenzel, G.; Speak, T. H.; Changala, P. B.; Willis, R. H. J.; Burkhardt, A. M.; Zhang, S.; Bergin, E. A.; Byrne, A. N.; Charnley, S. B.; Fried, Z. T. P.; et al. Detections of interstellar aromatic nitriles 2-cyanopyrene and 4-cyanopyrene in TMC-1. *Nat. Astron.* **2024**, 262-270.

(15) Holt, J. K.; Park, H. G.; Wang, Y.; Stadermann, M.; Artyukhin, A. B.; Grigoropoulos, C. P.; Noy, A.; Bakajin, O. Fast Mass Transport Through Sub-2-Nanometer Carbon Nanotubes. *Science* **2006**, *312*, 1034-1037.

(16) Ostrowski, J. H.; Eaves, J. D. The tunable hydrophobic effect on electrically doped graphene. *J. Phys. Chem. B.* **2014**, *118*, 530-536.

(17) Strong, S. E.; Eaves, J. D. Atomistic Hydrodynamics and the Dynamical Hydrophobic Effect in Porous Graphene. *J. Phys. Chem. Lett.* **2016**, *7*, 1907-1912.

(18) Ali, I.; Zenab Hasan, S.; Garcia, H.; Danquah, M. K.; Imanova, G. Recent advances in graphene-based nano-membranes for desalination. *Chem. Eng. J.* **2024**, *483*, 149108.

(19) McKenzie, S.; Kang, H. C. Squeezing water clusters between graphene sheets: energetics, structure, and intermolecular interactions. *Phys. Chem. Chem. Phys.* **2014**, *16*, 26004-26015.

(20) Lemmens, A. K.; Gruet, S.; Steber, A. L.; Antony, J.; Grimme, S.; Schnell, M.; Rijs, A. M. Far-IR and UV spectral signatures of controlled complexation and microhydration of the polycyclic aromatic hydrocarbon acenaphthene. *Phys. Chem. Chem. Phys.* **2019**, *21*, 3414-3422.

(21) Loru, D.; Steber, A. L.; Pinacho, P.; Gruet, S.; Temelso, B.; Rijs, A. M.; Pérez, C.; Schnell, M. How does the composition of a PAH influence its microsolvation? A rotational spectroscopy study of the phenanthrene–water and phenanthridine–water clusters. *Phys. Chem. Chem. Phys.* **2021**, *23*, 9721-9732.

(22) Pérez, C.; Steber, A. L.; Rijs, A. M.; Temelso, B.; Shields, G. C.; Lopez, J. C.; Kisiel, Z.; Schnell, M. Corannulene and its complex with water: a tiny cup of water. *Phys. Chem. Chem. Phys.* **2017**, *19*, 14214-14223.

(23) Steber, A. L.; Pérez, C.; Temelso, B.; Shields, G. C.; Rijs, A. M.; Pate, B. H.; Kisiel, Z.; Schnell, M. Capturing the elusive water trimer from the stepwise growth of water on the surface of the polycyclic aromatic hydrocarbon acenaphthene. *J. Phys. Chem. Lett.* **2017**, *8*, 5744-5750.

(24) Knurr, B. J.; Adams, C. L.; Weber, J. M. Infrared Spectroscopy of Hydrated Naphthalene Cluster Anions. *J. Chem. Phys.* **2012**, *137*, 104303.

(25) Rossich Molina, E.; Xu, B.; Kostko, O.; Ahmed, M.; Stein, T. A combined theoretical and experimental study of small anthracene–water clusters. *Phys. Chem. Chem. Phys.* **2022**, *24*, 23106-23118.

(26) Chatterjee, K.; Dopfer, O. Infrared spectroscopy of hydrated polycyclic aromatic hydrocarbon cations: naphthalene$^+$–water. *Phys. Chem. Chem. Phys.* **2017**, *19*, 32262-32271.

(27) Chatterjee, K.; Dopfer, O. Microhydration of PAH$^+$ cations: evolution of hydration network in naphthalene$^+$-$(H_2O)_n$ clusters ($n \leq 5$). *Chem. Sci.* **2018**, *9*, 2301-2318.

(28) Lemmens, A. K.; Ferrari, P.; Loru, D.; Batra, G.; Steber, A. L.; Redlich, B.; Schnell, M.; Martinez-Haya, B. Wetting of a hydrophobic surface: Far-IR action spectroscopy and dynamics of microhydrated naphthalene. *J. Phys. Chem. Lett.* **2023**, *14*, 10794-10802.

(29) Loru, D.; Sun, W.; Nootebos, H.; Steber, A. L.; Ferrari, P.; Schnell, M. Probing the structure and dynamics of the heterocyclic PAH xanthene and its water complexes with infrared and microwave spectroscopy. *Phys. Chem. Chem. Phys.* **2024**, *26*, 25341-25351.

(30) Salzmann, H.; Rasmussen, A. P.; Eaves, J. D.; Weber, J. M. Competition between Water–Water Hydrogen Bonds and Water–π Bonds in Pyrene–Water Cluster Anions. *J. Phys. Chem. A.* **2024**, *128*, 2772-2781.

(31) Domingos, S. R.; Martin, K.; Avarvari, N.; Schnell, M. Water Docking Bias in [4]Helicene. *Angew. Chem., Int. Ed.* **2019**, *58*, 11257-11261.

(32) Loru, D.; Steber, A. L.; Pérez, C.; Obenchain, D. A.; Temelso, B.; López, J. C.; Schnell, M. Quantum tunneling facilitates water motion across the surface of phenanthrene. *J. Am. Chem. Soc.* **2023**, *145*, 17201-17210.

(33) LeMessurier, N.; Salzmann, H.; Leversee, R.; Weber, J. M.; Eaves, J. D. Water–Hydrocarbon Interactions in Anionic Pyrene Monohydrate. *J. Phys. Chem. B.* **2024**, *128*, 3200-3210.

(34) Lemmens, A. K.; Rap, D. B.; Thunnissen, J. M. M.; Mackie, C. J.; Candian, A.; Tielens, A. G. G. M.; Rijs, A. M.; Buma, W. J. Anharmonicity in the mid-infrared spectra of polycyclic aromatic hydrocarbons: molecular beam spectroscopy and calculations. *A&A* **2019**, *628*, A130.

(35) Liu, K.; Loeser, J. G.; Elrod, M. J.; Host, B. C.; Rzepiela, J.; Pugliano, N.; Saykally, R. J. Dynamics of structural rearrangements in the water trimer. *J. Am. Chem. Soc.* **1994**, *116*, 3507-3512.

(36) Pugliano, N.; Saykally, R. Measurement of quantum tunneling between chiral isomers of the cyclic water trimer. *Science* **1992**, *257*, 1937-1940.

(37) Cruzan, J.; Braly, L.; Liu, K.; Brown, M.; Loeser, J.; Saykally, R. Quantifying hydrogen bond cooperativity in water: VRT spectroscopy of the water tetramer. *Science* **1996**, *271*, 59-62.

(38) Cruzan, J. D.; Braly, L. B.; Liu, K.; Brown, M. G.; Loeser, J. G.; Saykally, R. J. Quantifying Hydrogen Bond Cooperativity in Water: VRT Spectroscopy of the Water Tetramer. *Science* **1996**, *271*, 59-62.

(39) Wolke, C. T.; Menges, F. S.; Tötsch, N.; Gorlova, O.; Fournier, J. A.; Weddle, G. H.; Johnson, M. A.; Heine, N.; Esser, T. K.; Knorke, H.; et al. Thermodynamics of Water Dimer Dissociation in the Primary Hydration Shell of the Iodide Ion with Temperature-Dependent Vibrational Predissociation Spectroscopy. *J. Phys. Chem. A.* **2015**, *119*, 1859-1866.

(40) Ayotte, P.; Bailey, C. G.; Weddle, G. H.; Johnson, M. A. Vibrational Spectroscopy of Small $Br^-\cdot(H_2O)_n$ and $I^-\cdot(H_2O)_n$ Clusters: Infrared Characterization of the Ionic Hydrogen Bond. *J. Phys. Chem. A.* **1998**, *102*, 3067-3071.

(41) Hammer, N.; Roscioli, J.; Johnson, M.; Myshakin, E.; Jordan, K. Infrared spectrum and structural assignment of the water trimer anion. *J. Phys. Chem. A.* **2005**, *109*, 11526-11530.

(42) Shin, J.-W.; Hammer, N. I.; Headrick, J. M.; Johnson, M. A. Preparation and photoelectron spectrum of the 'missing' $(H_2O)_4^-$ cluster. *Chemical Physics Letters* **2004**, *399*, 349-353.

(43) Weber, J. M. A pulsed ion source for the preparation of metal containing cluster anions using supersonic entrainment of laser vaporized metal. *Rev. Sci. Instrum.* **2005**, *76*, 043301.

(44) *Origin Pro "Version 2021"*; Northampton, MA, USA, 2021.

(45) Wallace, W. E. Infrared Spectra. In *NIST Chemistry WebBook, NIST Standard Reference Database Number 69*; National Institute of Standards and Technology, https://webbook.nist.gov/chemistry, accessed 08/20/2024.

(46) Frisch, M. J.; Trucks, G. W.; Schlegel, H. B.; Scuseria, G. E.; Robb, M. A.; Cheeseman, J. R.; Scalmani, G.; Barone, V.; Petersson, G. A.; Nakatsuji, H.; et al. Gaussian 16 Rev. C.01. **2016**.

(47) Chai, J. D.; Head-Gordon, M. Systematic optimization of long-range corrected hybrid density functionals. *J. Chem. Phys.* **2008**, *128*, 084106.

(48) Krishnan, R.; Binkley, J. S.; Seeger, R.; Pople, J. A. Self-consistent molecular orbital methods. XX. A basis set for correlated wave functions. *J. Chem. Phys.* **1980**, *72*, 650-654.

(49) McLean, A. D.; Chandler, G. S. Contracted Gaussian basis sets for molecular calculations. I. Second row atoms, Z=11–18. *J. Chem. Phys.* **1980**, *72*, 5639-5648.

(50) Becke, A. D. Density-functional thermochemistry. III. The role of exact exchange. *J. Chem. Phys.* **1993**, *98*, 5648-5652.

(51) Besler, B. H.; Merz Jr., K. M.; Kollman, P. A. Atomic charges derived from semiempirical methods. *J. Comput. Chem.* **1990**, *11*, 431-439.

(52) Singh, U. C.; Kollman, P. A. An approach to computing electrostatic charges for molecules. *J. Comput. Chem.* **1984**, *5*, 129-145.

(53) Schiedt, J.; Weinkauf, R. Photodetachment photoelectron spectroscopy of perylene and CS2: two extreme cases. *Chem. Phys. Lett.* **1997**, *274*, 18-22.

(54) Xantheas, S. S.; Dunning, T. H., Jr. Ab initio studies of cyclic water clusters $(H_2O)_n$, n=1–6. I. Optimal structures and vibrational spectra. *J. Chem. Phys.* **1993**, *99*, 8774-8792.

(55) Zhang, B.; Yu, Y.; Zhang, Z.; Zhang, Y.-Y.; Jiang, S.; Li, Q.; Yang, S.; Hu, H.-S.; Zhang, W.; Dai, D.; et al. Infrared Spectroscopy of Neutral Water Dimer Based on a Tunable Vacuum Ultraviolet Free Electron Laser. *J. Phys. Chem. Lett.* **2020**, *11*, 851-855.

(56) Ramos-Cordoba, E.; Lambrecht, D. S.; Head-Gordon, M. Charge-transfer and the hydrogen bond: Spectroscopic and structural implications from electronic structure calculations. *Faraday Disc.* **2011**, *150*, 345-362.

(57) Mao, Y.; Horn, P. R.; Head-Gordon, M. Energy decomposition analysis in an adiabatic picture. *Phys. Chem. Chem. Phys.* **2017**, *19*, 5944-5958.

(58) Lide, D. R. *CRC handbook of chemistry and physics*; CRC press, 2004.

(59) Ayotte, P.; Weddle, G. H.; Johnson, M. A. An infrared study of the competition between hydrogen-bond networking and ionic solvation: Halide-dependent distortions of the water trimer in the $X^{-}\cdot(H_2O)_3$, (X=Cl, Br, I) systems. *J. Chem. Phys.* **1999**, *110*, 7129-7132.

TOC Graphic